Journal of Applied Polymer Science

Effect of the Graphite Nanoplatelet Size on the Mechanical, Thermal, and Electrical Properties of Polypropylene/Exfoliated Graphite Nanocomposites

E. V. Kuvardina,[1] L. A. Novokshonova,[1] S. M. Lomakin,[2] S. A. Timan,[1] I. A. Tchmutin[3]

[1]Semenov Institute of Chemical Physics, Russian Academy of Sciences, Kosygin Street, 4, Moscow 119991 Russia

[2]Emanuel Institute of Biochemical Physics, Kosygin Street, 4, Moscow 119334 Russia

[3]Open Joint Stock Company Industrial Park "Slava", Nauchnyi Passage, 20/2, Moscow 117246 Russia

Correspondence to: E. V. Kuvardina (E-mail: janekuvardina@yandex.ru)

ABSTRACT: Polypropylene (PP)/exfoliated graphite nanoplatelet (xGnP) nanocomposites with various intrinsic aspect ratios of graphite nanoplatelets (GnPs; large and small in diameter) were prepared by a melt-mixing procedure. Transmission electron microscopy showed that all types of xGnP were well-dispersed in the polymer matrix. The effects of the dimensions and loading of the xGnPs on the morphology, mechanical reinforcement, and electrical properties of PP/xGnP were studied. A differential scanning calorimetry study of the PP/xGnP morphology indicated that all types of xGnP additives were heterogeneous nucleation sites for PP crystallization. Tensile testing, DMA, and thermogravimetric analysis of PP/xGnPs with different types of GnP additives showed enhancements in their mechanical properties, heat resistance, and thermal stability compared to plain PP. We also found a significant increase in the conductivity of PP/xGnP. The PP/xGnP with a large diameter of GnPs demonstrated the lowest percolation threshold, equal to 4 vol % of the xGnP loading. The mechanical properties were estimated by means of micromechanical modeling. © 2012 Wiley Periodicals, Inc. J. Appl. Polym. Sci. 000: 000–000, 2012

KEYWORDS: conducting polymers; mechanical properties; polyolefins; structure–property relations

Received 26 April 2012; accepted 22 June 2012; published online
DOI: 10.1002/app.38237

INTRODUCTION

The discovery of graphene in 2004 stimulated a number of investigations of its fabrication.[1–5] The unique properties of the new material, such as its high electrical conductivity (~ 6000 S/cm) and tensile strength (~ 1 TPa) make it advantageous (perspective) for use in a wide range of applications[6–13] and in compositions with polymers.[14–17] However, nowadays, there is an important problem with graphene mass production. All of the diverse developed approaches can be divided into two general directions, top-down and bottom-up, where in the first case, we try to extract a monolayer from original graphite,[3–5] and in the second, we try to create a supramolecular aromatic structure from low-mass-weight units.[1–2] At this time, the top-down approach is more technological and developed. It can be performed by both physical and chemical methods.[18–20] However, the main product that has resulted is a stack of graphene layers, which are referred to as *graphite nanoplatelets* (GnPs).[21–23] The physical properties of such platelets are lower than those of graphene. Nevertheless, the importance of such a filler is still high because of its higher stiffness and electrical conductivity compared to those of graphite and also its lower cost due to its nanosize. In this study, we observed two types of nanoplatelets and the effects of the platelet aspect ratio on the structure and mechanical, thermal, and electrical properties of polypropylene (PP)/exfoliated graphite nanoplatelet (xGnP) nanocomposites in comparison with conventional fillers.

We also estimated the mechanical properties of PP/xGnP with the aid of micromechanical modeling. We applied two theoretical models: the Mori–Tanaka model[24] for discs and the finite element model of thin inclusions (MTI).[25] It is well known that self-consistent analytic approaches for composite mechanics[26,27] are applicable for predicting the hardening of polymers reinforced by rigid particles of highly asymmetric shape. Self-consistent techniques can be implemented because of Eshelby's solution[28] concerning the task of deformation of an elastic medium with a single ellipsoidal inclusion uniformly loaded at infinity. This solution guarantees that the shapes of the inclusion are preserved but its orientation and dimensions are changed. However, one intuitively expects significant bending in strongly oblong or oblate ellipsoidal inclusions randomly

Table I. Main Characteristics of the xGnPs

xGnP type	*d* (nm)	Initial *L* (μm)	*L* after sonication (μm)	*L*/*d*	ρ (g/cm^3)	$\sigma_{dc} \times 10^{-3}$ (S/cm)
xGnP(5)	10	5	1	100	1.8	490
xGnP(10)	10	10	2	200	1.8	230

arranged in an elastic medium. Hence, the effective moduli of such disordered heterogeneous materials predicted by the Mori–Tanaka model are inevitably overestimated. At the same time, the complicated numerical approach allows one to take into account the influence of bending deformation on the composite material effective moduli. Therefore, to provide numerical calculations of the values of the effective moduli, simplified assumptions are suggested, for example, MTI.

EXPERIMENTAL

Materials

Isotactic PP (Moscow Naphta Processing Plant, Russia) with a melt flow index of 0.6 g/10 min (2.16 kg, 230°C) was used as the matrix polymer ($M_w = 6.3 \times 10^5$ g/mol, $M_w/M_n = 3.5$).

xGnPs were supplied by XG Sciences Company (USA, MI, East Lansing). xGnPs were prepared by the microwave expansion of graphite oxide. Two types of xGnPs with different intrinsic diameter (*d*), length (*L*), and aspect ratio (*L*/*d*; Table I) values were investigated as nanosized fillers. The filler data presented in Table I were obtained by AFM and TEM.

Processing

Preparation of the Nanocomposites. The composites were prepared by melt mixing in a two-roller mixing chamber (Institute of Chemical Physics, Moscow, Russia) at 190°C and with a rotor rotation speed of 90 rpm. First, PP was melt-blended with stabilizers of the thermooxidative degradation (0.3 wt % of topanol and 0.5 wt % of dilauriltiodipropionate) for 3 min. The xGnPs were then added slowly over 3 min, and the mixture was compounded for 15 min. The nanoparticle loadings were in the range 0.5–10 vol % (1–20 wt %). For comparison, composites based on conventional fillers, such as carbon black and graphite, and pristine PP were also processed in the mixer.

Specimen Preparation. The specimens, as 0.5 mm thick plates, for morphological and mechanical testing were compression-molded. The molding procedure involved heating at 190°C for 5 min without applied pressure and then heating for 5 min under pressure (10 MPa). The mold was cooled down by water to 90°C under pressure.

Structural Characterization (Methods/Characterization Techniques)

Transmission Electron Microscopy. The dispersion and distribution of xGnPs in the PP matrix were examined by transmission electron microscopy (TEM) with the use of a LEO-912 AB Omega instrument (Germany) at an accelerating voltage of 100 kV. Ultrathin sections of the composite specimens, with a thickness of about 100 nm, were prepared with a Reichert-Jung Ultracut ultramicrotome with a diamond knife.

Scanning Electron Microscopy. The dispersion of nanoparticles in the polymer matrix was analyzed with a JSM-35 scanning electron microscope (JEOL Ltd., Tokyo, Japan). The samples were fractured in liquid nitrogen and then covered with a thin gold layer to prevent charging.

Differential Scanning Calorimetry (DSC). The crystallization and melting behavior of the unfilled PP and PP matrix in the presence of xGnPs were investigated with a differential scanning calorimeter (DSC-204 F1, Netzsch, Germany) under a nitrogen atmosphere. Heating and nonisothermal crystallization DSC experiments were carried out in the 25–180°C range at a rate of 10°C/min. Thermograms were used to determine the peak melting temperature, enthalpy of melting, and temperature of crystallization. The specific heat flow from the melting peak (W/g) was corrected for the mass of PP in the nanocomposite. The PP–matrix crystallinity in the nanocomposites was calculated with the value of melting enthalpy and for 100% crystalline PP was 209 J/g.[29]

Mechanical Properties

Tensile Testing. For mechanical testing, dumbbell specimens with dimensions of 30 × 5 × 0.5 mm^3 were cut from hot-pressed films. Uniaxial tensile testing of the composites was carried out with a tensile testing machine (Instron-1122) with a crosshead speed of 20 mm/min (0.67 min^{-1}) at room temperature. The elastic modulus, yield stress and strain, stress, and

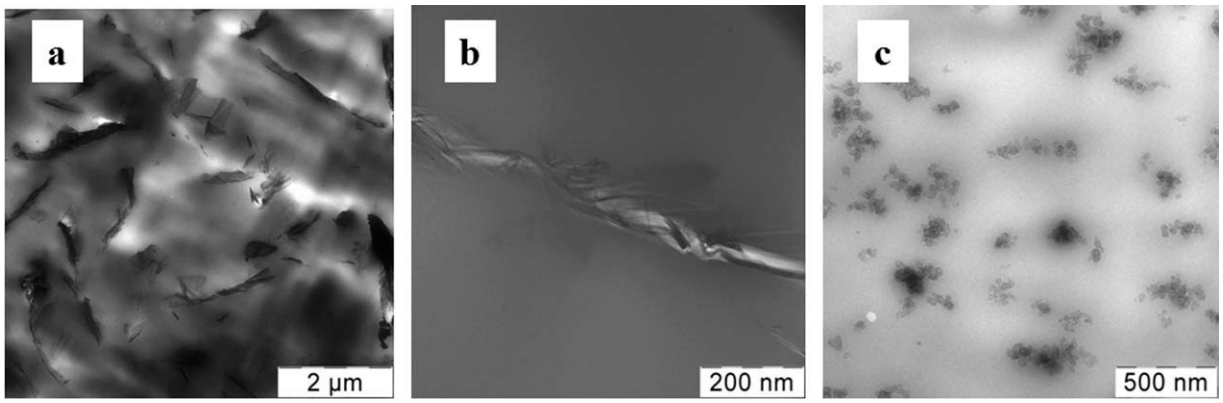

Figure 1. TEM photos of the (a) 10 vol % PP/xGnP nanocomposite, (b) spun platelet of xGnP, and (c) 2.5 vol % PP/carbon black composite.

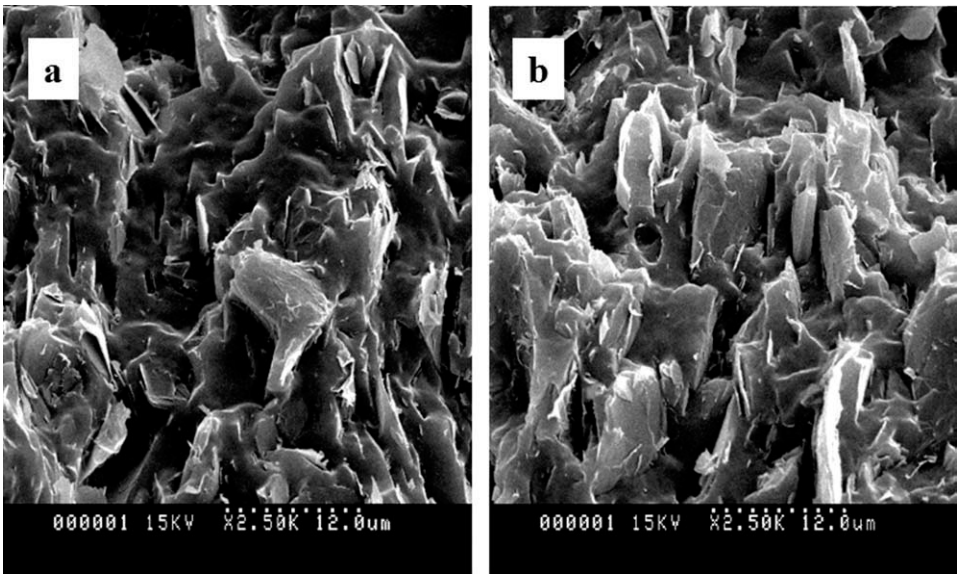

Figure 2. SEM photos of (a) PP/xGnP(5) and (b) PP/xGnP(10) nanocomposites.

elongation at break were determined from the stress–strain diagrams. The average values were calculated from eight runs for each specimen.

Dynamic Mechanical Analysis. For the dynamic mechanical measurements, an analyzer DMA 242 C/1/F (Netzsch, Germany) was applied. Bar shaped specimens of about 20 mm x 5 mm x 0.5 mm were cut from compression-molded sheets. Experiments were performed in the tensile mode at a frequency of 1 Hz. The samples were analyzed by dynamic strain amplitude of 0.2% in the temperature range −60 to 160°C under constant heating rate of 2°C/min. The storage modulus (E') and mechanical loss factor (tan δ) were determined as functions of temperature.

Thermal Properties

Thermogravimetric analysis (TGA) was conducted with a thermomicrobalance (TG 209 F1 Iris, Netzsch) under dynamic heating conditions in an air atmosphere. The samples weighed about 5–8 mg. The analysis was carried out at a heating rate of 20°C/min up to 1000°C.an

Electrical Properties (Conductivity and Dielectric Properties)

The direct-current conductivity (σ_{dc}) parallel to the sample plane was measured in this study. Room-temperature σ_{dc} with accuracy of ±5% was measured by the four-probe method. Copper wire was used as the electrode material, and silver adhesive, with a conductivity of 10^4 S/cm, was used to decrease the contact resistance.

RESULTS AND DISCUSSION

Morphology of the PP Nanocomposites

Transmission Electron Microscopy. Structural investigation of the GnPs was carried out by transmission electron microscopy and DSC. The photographs obtained by transmission electron microscopy are shown on Figure 1. It can be seen [Figure 1(a)]

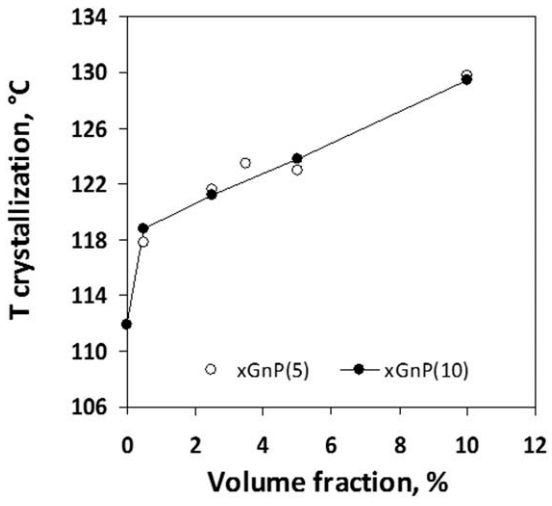

Figure 3. Crystallization temperature (T) of PP versus filler loading.

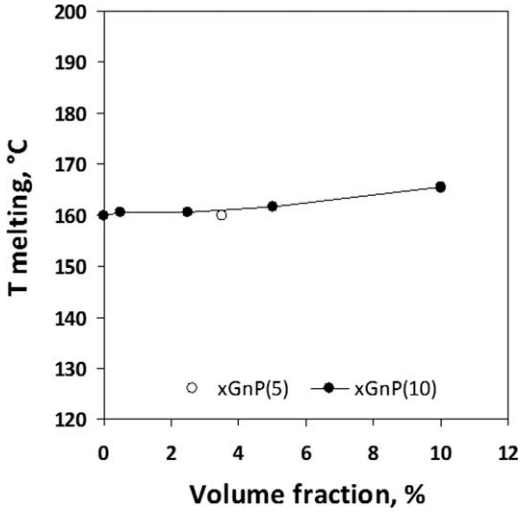

Figure 4. Melting temperature (T) of PP versus filler loading.

Applied Polymer SCIENCE

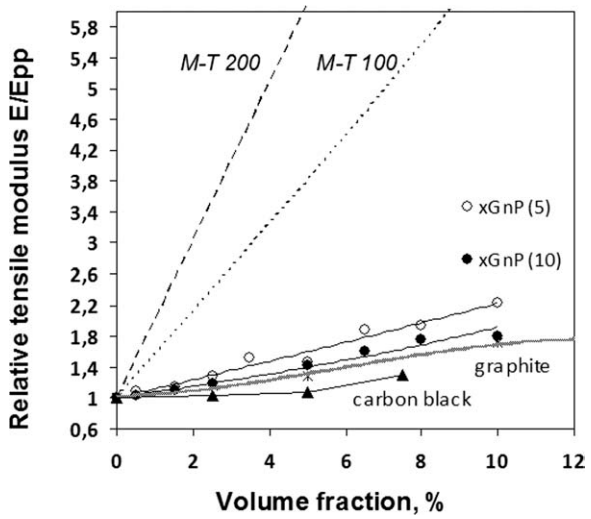

Figure 5. Experimental and calculated by the Mori–Tanaka model (for particles aspect ratios 100 and 200) E/E_{pp} versus filler loading.

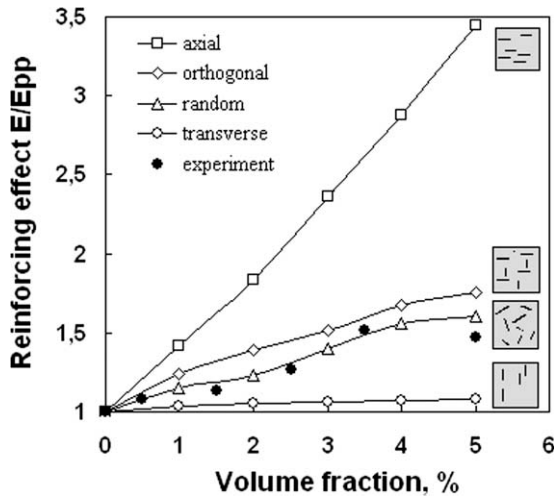

Figure 7. E/E_{pp} versus filler loading (FEM and experimental dependencies).

that the GnPs were well-dispersed, even at a rather high volume fraction (~10 vol %). However, at larger extents, we noticed [Figure 1(b)] that the nanoplatelets tended to spin, wrinkle, and form an ellipsoid-like shape. The comparative TEM photo [Figure 1(c)] of the carbon black-based composite showed that spherical particles of carbon black also dispersed quite uniformly while forming chainlike structures.

Scanning Electron Microscopy. Figure 2 presents the lower magnification SEM photos of nanocomposites based on GnPs of both types. It can be seen that the distribution of nanoparticles on the fractured surface of nanocomposites samples. Furthermore, we observed the brittle character of the sample fracture.

DSC. From the thermal diagrams, we plotted the volume fraction dependencies of the crystallization temperature (Figure 3) and melting temperature (Figure 4). One can see that both types of nanoplatelets showed a nucleating effect, which led to an increase in the crystallization temperature. At a volume fraction of 10 vol %, the crystallization temperature rose by 18°C. However, platelike particles did not on the size of spherulites; this could be seen from the invariant behavior of the melting temperature at different filler loadings.

Mechanical Properties

Tensile Testing. The high aspect ratio and huge surface area of carbon nanofillers suggested significant improvement in the mechanical properties of the nanocomposites. The dependencies of the filler reinforcing effect (E/E_{pp}) from the filler volume fraction indicated that the xGnP effectiveness was higher than that of conventional carbon fillers (e.g., graphite and carbon black) in a wide range of concentrations (Figure 5). Spherical particles, such as carbon black, exhibited the lowest reinforcement. The reinforcing efficiency of xGnP(5) was slightly higher than that of xGnP(10), with a larger nanoplatelets diameter.

To estimate the limits of theoretical reinforcement by carbon nanoplatelets, we used Mori–Tanaka predictions.[26,27] The Eshelby tensor[30] for round-shape thin discs (oblate ellipsoids) with aspect ratios corresponding to those experimentally measured (100 and 200) was applied to calculate the effective moduli. The Poisson ratio used was 0.25, and the ratio of filler modulus to matrix modulus was 1000. The resulting stiffness corresponded to a transversal isotropic material with ordered inclusions. To estimate

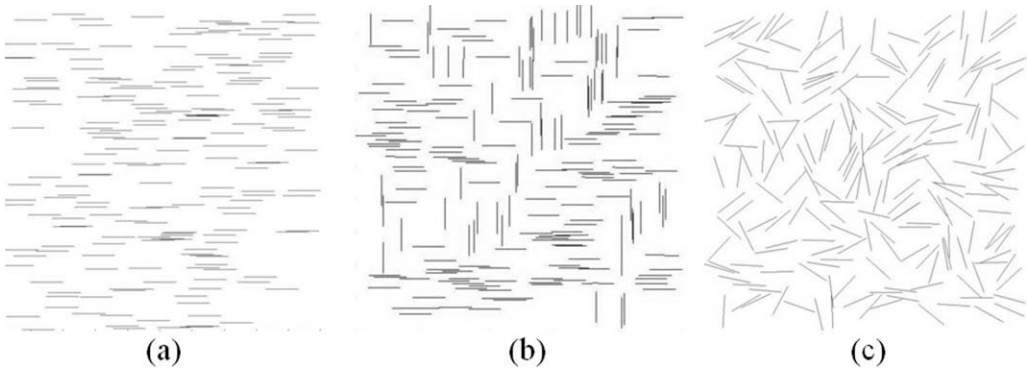

Figure 6. RVEs of the structures containing chaotically arranged asymmetric inclusions: (a) unidirectional, (b) oriented in orthogonal directions, and (c) chaotically oriented.

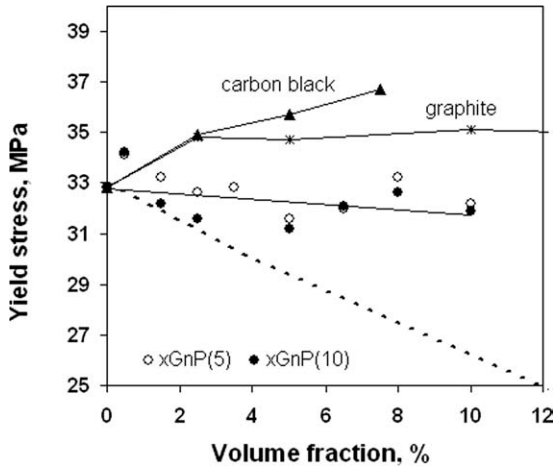

Figure 8. Composite yield stress versus filler loading.

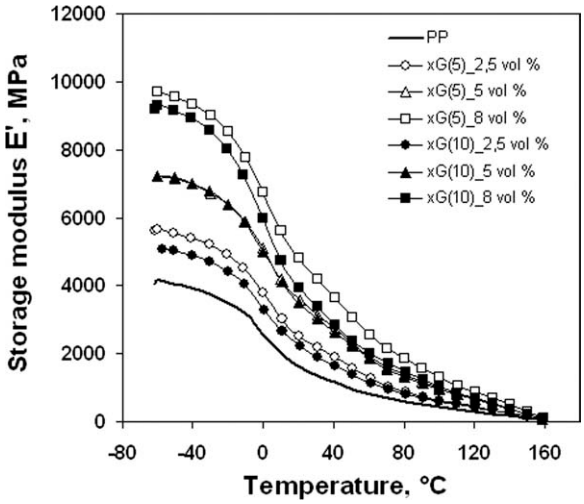

Figure 10. E' values of the composites versus temperature.

the properties of the material with a chaotic inclusion arrangement, it was necessary to perform averaging in all directions.[31]

Figure 5 shows that the calculated values of reinforcing effect according to the Mori–Tanaka model were far from the experimental data. A numerical simulation of composite rigidity was carried out with the aid of simplified MTI to determine the cause of this spread of results.[25] MTI is intended to describe the mechanical properties of a polymer filled with high asymmetric particles (platelets or fibers). The main assumption of the model consisted of an idea that the inclusions with high aspect ratio could be imagined as thin plates or beams with deformational properties described by longitudinal tensile/compression moduli and bending rigidity. This notion allowed us to calculate the elastic and viscoelastic properties of the composites with disordered spatial and orientational arrangements of the inclusions for a sufficiently large representative volume element (RVE; Figure 6).

Figure 7 shows the calculated relative tensile modulus dependencies from the filler loading for different filler arrangements. There are also comparative data of the experimental relative tensile modulus, where one can see that our tensile test results were well described by the case of chaotic filler arrangement. It is noteworthy that our results were well described by this model on the assumption of absolutely flexible plates. This fact proved that consideration of asymmetric inclusion bending rigidity is a matter of importance for the calculation of effective composite stiffness.

The yield stress dependence on the filler loading of the PP/xGnP nanocomposites is shown on Figure 8. The yield stress of the composites with GnPs slightly decreased with their loading; this might have been caused by particle detachment under the yield stress conditions and could be described according to the model with minimum effective stressed area (Figure 8, dashed line).[32] For the composites with conventional carbon fillers, the yield stress tended to rise. It was possible that some surface adhesion with the polymer matrix existed and was described by the model with absolute filler adhesion.

Further treatment of the stress–strain dependencies showed that the PP composites with different types of carbon fillers exhibited

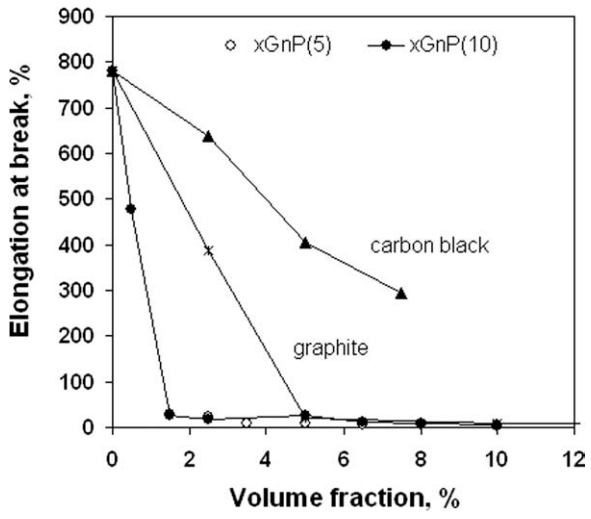

Figure 9. Composite elongation at break versus filler loading.

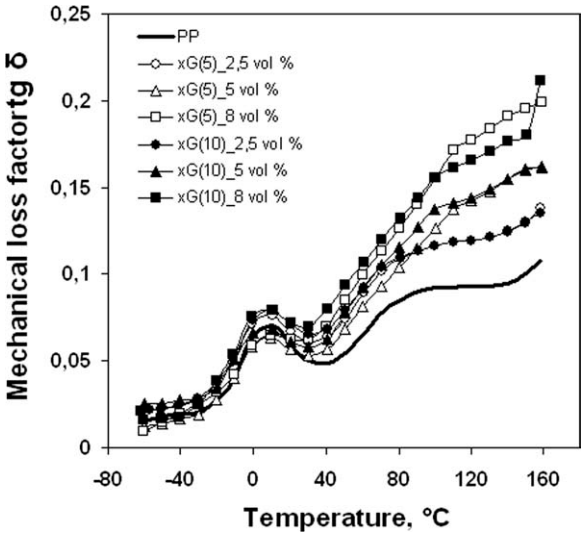

Figure 11. Tan δ of the composites versus temperature.

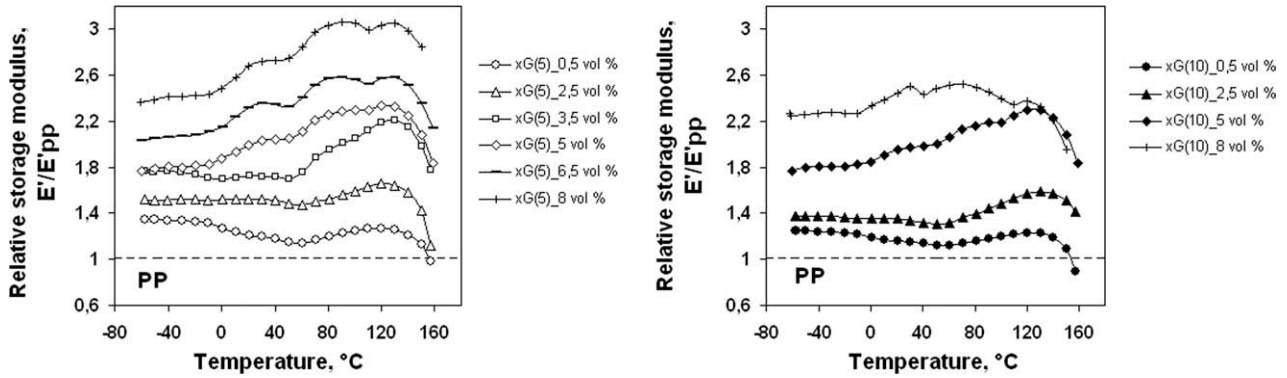

Figure 12. Relative storage modulus (E') values of the composites with (a) xGnP(5) and (b) xGnP(10) versus temperature.

different deformation behaviors (Figure 9). In a range of fillers, carbon black, graphite, and GnPs, the deformation characteristics decreased. At a volume fraction of 2.5%, the composites with xGnPs exhibited brittle fracture, whereas the composites with carbon black revealed plastic behavior. Thus, the filler loading and aspect ratio determined the type of composite fracture.

Dynamical Mechanical Analysis. To assess the heat resistance of the materials, DMA was carried out in the temperature range from −60 to 160°C. The temperature dependencies of E' and tan δ are presented on Figures 10 and 11, respectively. The values of relative E' were also calculated from the E' dependencies (Figure 12).

Apparently, the values of E' for the PP/xGnP nanocomposites rose with increasing filler volume fraction (Figure 10). The E' values of the composites with xGnP with lower diameters was slightly higher than those of the composites with xGnP with larger diameters.

The relaxation behavior was investigated by analysis of the temperature dependencies of the composite tan δ. The glass-transition temperature of PP did not change in the presence of either type of xGnP filler (Figure 11). At the same time, the high-temperature loss peak of the composites, which were characterized by segmental mobility in the crystalline regions, tended to shift in a higher temperature area.

On the temperature dependencies of relative E' the reinforcing effects of the nanoplatelets are presented (Figure 12). Evidently, the GnPs enhanced the stiffness of the composites in a whole temperature range. Figure 12 shows that for all filler loadings, the reinforcing effect of xGnP(5) with less length was slightly higher than that of xGnP(10). At higher temperatures, the values of the relative modulus of the composites retained higher values, which indicated an increase in the material's heat resistance. The temperature increase from 25 to 100°C led to an increase in the filler reinforcement effect from 2 to 2.3 at 5 vol %.

Thermal Properties (TGA)

The diverse behavior of the PP and PP/xGnP nanocomposites with 1 and 5 wt % (0.5 and 2.5 vol %) xGnP showed that the influence of xGnPs on the thermooxidation process resulted in a higher thermooxidative stability in the PP/xGnP nanocomposites. The thermogravimetric (TG) and differential thermogravimetry (DTG) curves of the PP and PP/xGnP nanocomposites are presented on Figure 13.

Detailed analysis of TGA graphs allowed us to claim that the thermooxidative stability increased was achieved even with the addition of 1 wt % xGnP to PP and further increased with

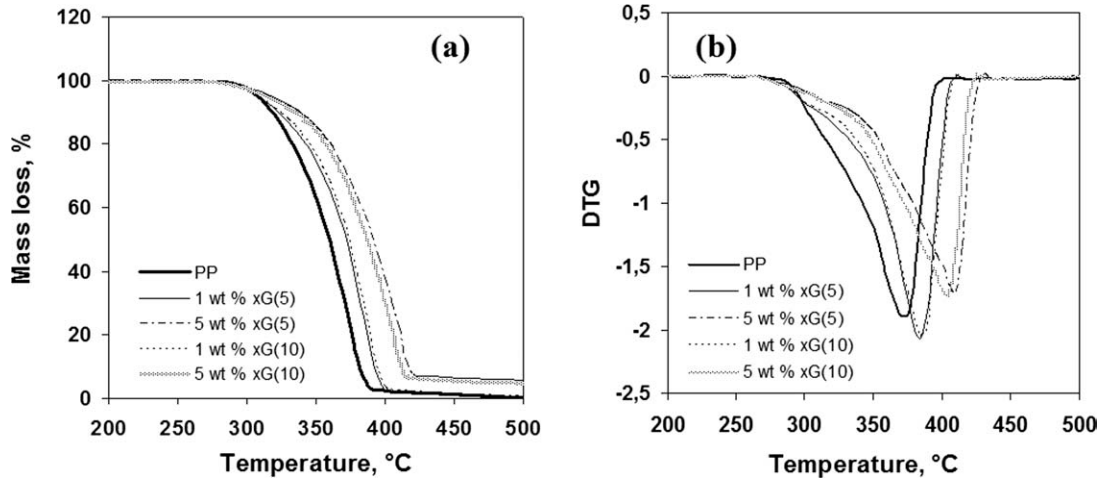

Figure 13. (a) TG and (b) DTG curves of the PP and PP/xGnP nanocomposites obtained in an air atmosphere.

Table II. Values of the Onset Decomposition Temperatures (T_{on}) and Temperatures of the Maximum Mass Loss Rates (T_{max}) for the PP and PP/xGnP Nanocomposites Obtained from TGA

Sample	T_{on} (°C)	T_{max} (°C)
PP	333	371
PP/xGnP(5) 1 wt %	333	381
PP/xGnP(10) 1 wt %	348	385
PP/xGnP(5) 5 wt %	346	409
PP/xGnP(10) 5 wt %	358	406
PP/xGnP(5) 10 wt %	372	409
PP/xGnP(10) 10 wt %	374	406
PP/xGnP(5) 16 wt %	381	421
PP/xGnP(10) 16 wt %	375	409

the filler loading. Table II shows the comparative results for the onset decomposition temperatures and the temperatures of the maximum mass loss rates for the PP and PP/xGnP nanocomposites in an air atmosphere with the different types and concentrations of xGnP.

Supposedly, the observed increase in the thermal stability of the PP/xGnP nanocomposites was associated with the shielding effect of GnPs forming the flocculated layer on the surface of the PP/xGnP nanocomposites during the thermal degradation process. This graphite layer, which had physical integrity, was effective in reducing the PP thermal oxidation and volatilization of the degradation products.

Electrical Properties

The concentration dependencies of σ_{dc} of the PP composites with xGnP(5) and xGnP(10) are plotted in Figure 14. It can be seen that all of the PP/xGnP composites exhibited typical percolation behavior. The introduction of xGnPs to PP increased the conductivity of the resulting composites by more than 10 orders of magnitude. According to Figure 14, the percolation threshold value for the composites based on xGnP(5) was 6 vol %, and it decreased to 4 vol % for composites with xGnP(10) with a larger aspect ratio.

In Figure 14, the σ_{dc} concentration dependencies for the nanocomposites are also compared with those of composites with traditional carbon fillers. As the conductivity of the GnPs was usually about 10^2 S/cm, for comparison, we used data for PP composites based on carbon fillers with close σ_{dc} values: (1) graphite EUZ-M (flake-shaped particles with $L/d \approx 10$ and $\sigma_{dc} = 10^2$ S/cm) and (2) carbon black Vulcan XC 72R (chain structure clusters with $L/d \approx 30$ and $\sigma_{dc} = 10^2$ S/cm). As can be seen, the percolation threshold for the PP/xGnP composite was lower than those for composites based on graphite EUZ-M ($\Phi_c = 9.5$ vol %) and carbon black Vulcan XC 72R ($\Phi_c = 6.5$ vol %).

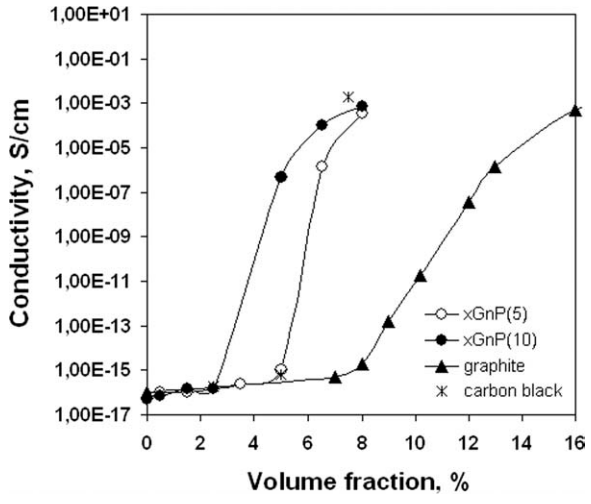

Figure 14. Conductivity of the PP composites with different types of fillers versus filler loading.

CONCLUSIONS

The experimental results demonstrate that the PP nanocomposites with GnPs had enhanced mechanical and electrical properties and improved PP matrix thermal stability and heat resistance.

The rise in the thermal stability of the PP/xGnP nanocomposites. as compared with pristine PP, was associated with the shielding effect of GnPs forming the flocculated thermostable layer onto the surface of the PP/xGnP nanocomposites during the thermal degradation process; this depressed the volatilization of the PP degradation products.

Micromechanical modeling showed that the MTI theoretical model, which considered graphite particle bending, described E/E_{pp} in the PP/xGnP nanocomposites quite well.

ACKNOWLEDGMENTS

The authors thank the Ministry of Education and Science of the Russian Federation for financial support (contract number 11.519.11.3025). The authors thank Sergey S. Abramchuk from Moscow State University for great assistance in the transmission electron microscopy analysis.

REFERENCES

1. Eizenberg, M.; Blakely, J. M. *Surf. Sci.* **1979,** *82*, 228.
2. Aizawa, T.; Souda, R.; Otani, S.; Ishizawa, Y.; Oshima, C. *Phys. Rev. Lett.* **1990,** *64*, 768.
3. Novoselov, K. S.; Geim, A. K.; Morozov, S. V.; Jiang, D.; Zhang, Y.; Dubonos, S. V.; Grigorieva, I. V.; Firsov, A. A. *Science* **2004,** *306*, 666.
4. Lu, X.; Yu, M.; Huang, H.; Rouff, R. S. *Nanotechnology* **1990,** *10*, 269.
5. Berger, C.; Song, Z.; Li, X.; Wu, X.; Brown, N.; Naud, C.; Mayou, D.; Li, T.; Hass, J.; Marchenkov, A. N.; Conrad, E. H.; First, P. N.; de Heer, W. A. *Science* **2006,** *312*, 1191.
6. Allen, M. J.; Tung, V. C.; Kaner, R. B. *Chem. Rev.* **2010,** *110*, 132.
7. Sundaram, R. S.; Gomez-Navarro, C.; Balasubhramaniam, K.; Burghard, M.; Kern, K. *Adv. Mater.* **2008,** *20*, 3050.

8. Gomez-Navarro, C.; Weitz, R. T.; Bittner, A. M.; Scolari, M.; Mews,. A.; Burghard, M.; Kern, K. *Nano Lett.* **2007,** *7*, 3499.
9. Hirata, M.; Gotou, T.; Ohba, M. *Carbon* **2005,** *43*, 503.
10. Geim, A. K.; Novoselov, K. S. *Nat. Mater.* **2007,** *6*, 183.
11. Zhang, Y. B.; Tan, Y. W.; Stormer, H. L.; Kim, P. *Nature* **2005,** *438*, 201.
12. Wu, J.; Agrawal, M.; Becceril, H. A.; Bao, Z.; Liu, Z.; Chen, Y; Peumans, P. *ACS Nano* **2010,** *4*, 43.
13. Wang, X.; Zhi, L.; Mullen, K. *Nano Lett.* **2008,** *8*, 323.
14. Stankovich, S.; Dikin, D. A.; Dommett, G. H. B.; Kohlhaas, K. M.; Zimney, E. J.; Stach, E. A; Piner, R. D.; Nguyen, S. T.; Ruoff, R. S. *Nature* **2006,** *442*, 282.
15. Ansari, S.; Giannelis, E. P. *J. Polym. Sci. Part B: Polym. Phys.* **2009,** *47*, 888.
16. Ramanathan, T.; Abdala, A. A.; Stankovich, S.; Dikin, D. A.; Herrera-Alonso, M.; Piner, R. D.; Adamson, D. H.; Schniepp, H. C., Chen, X.; Ruoff, R. S.; Nguyen, S. T.; Aksay, I. A.; PrudHomme, R. K.; Brinson, L. C. *Nat. Nanotechnol.* **2008,** *3*, 327.
17. Kim, H.; Macosko, C. W. *Polymer* **2009,** *50*, 3797.
18. Park, S.; Ruoff, R. S. *Nat. Nanotechnol.* **2009,** *4*, 217.
19. Jang, B. Z.; Zhamu, A. J. *Mater. Sci.* **2008,** *43*, 5092.
20. McAllister, M. J.; Li, J.-L.; Adamson, D. H.; Schniepp, H. C.; Abdala, A. A.; Liu, J., Herrera-Alonso, M.; Milius, D. L.; Car, R.; Prud'homme, R. K.; Aksay, I. A. *Chem. Mater.* **2007,** *19*, 4396.
21. Lee, J. H.; Shin, D. W.; Makotchenko, V. G.; Nazarov, A. S.; Fedorov, V. E.; Kim, Y. H.; Choi, J.-Y.; Kim, J. M.; Yoo, J.-B. *Adv. Mater.* **2009,** *21*, 4383.
22. Fukushima, H. Ph.D. Thesis, Michigan State University, **2003.**
23. Kalaitzidou, K.; Fukushima, H.; Drzal, L. T. *Compos. Sci. Technol.* **2007,** *67*, 2045.
24. Mori, T.; Tanaka, K. *Acta Metall.* **1973,** *21*, 571.
25. Berlin, A. A.; Oshmyan, V. G.; Patlazhan, S. A.; Timan, S. A.; Shamaev, M. Y.; Khokhlov, A. R. *Polym. Sci. A* **2006,** *48*, 198.
26. Tandon, G. P.; Weng, G. J. *Polym. Compos.* **1984,** *5*, 327.
27. Tucker, C. L.; Liang, E. *Compos. Sci. Technol.* **1999,** *59*, 655.
28. Eshelby, J. D. *Proc. R. Soc. A* **1957,** *241*, 376.
29. Wunderlich, B. Macromolecular Physics; Academic: New York, **1976; Vol.** *2*.
30. Mura, T. Micromechanics of Defects in Solids; Martinus Nijhoff: Dordrecht, The Netherlands, **1987.**
31. Christensen, R. M. Mechanics of Composite Materials; Wiley: New York, **1979.**
32. Nicolais, L.; Narkis, M. *Polym. Eng. Sci.* **1971,** *11*, 194.